A CAR-BORNE SAR AND INSAR EXPERIMENT

Othmar Frey
Gamma Remote Sensing / Earth Observation & Remote Sensing, ETH Zurich
Switzerland
Email: frey@gamma-rs.ch

Charles L. Werner
Urs Wegmuller
Andreas Wiesmann
Gamma Remote Sensing
Switzerland

Daniel Henke
Christophe Magnard
Remote Sensing Laboratories
University of Zurich
Switzerland

***Abstract*—In this contribution, a car-borne SAR and InSAR experiment is described. The slope of a valley was imaged by means of a single-pass InSAR system mounted on a car driving on roads along the bottom of the valley. The GAMMA portable radar interferometer GPRI-II hardware with a modified antenna configuration was used for data acquisition. The experimental setup (1), SAR imagery focused along a slightly curved sensor trajectory (2), and first interferometric results (3) obtained using this configuration are presented.**

***Index Terms*—Synthetic aperture radar (SAR), ground-based SAR system, SAR imaging, SAR interferometry, car-borne SAR, CARSAR**

I. Introduction

Synthetic aperture radar interferometric techniques have been widely used to produce digital elevation models (DEMs) on a regional to global scale and to measure displacements in repeat-pass mode. Apart from spaceborne and airborne radars, also ground-based radar systems have appeared [1]–[4]. Ground-based radars add complementary advantages, such as timely in-situ measurements taken from a suitable viewpoint and repeatability of measurements in both time and space. They are therefore suitable to measure ground motion, to monitor land-slides, as well as to measure the topography of the illuminated area. In 2007, Gamma Remote Sensing developed a portable terrestrial real-aperture radar interferometer operating in the Ku-band at 17.2 GHz [1], [5]. The one-transmit-dual-receive configuration allows for a simultaneous acquisition of two SAR data sets in a single pass. Therefore, an interferometric evaluation of the illuminated scene is possible including rapidly decorrelating targets such as a forest. In addition, the atmospheric phase contributions cancel out and there is potentially no need to separate motion from topography for repeat-pass measurements. For the experiment described here the GPRI-II radar was employed in a modified configuration to enable a synthetic aperture radar acquisition mode from an agile platform.

II. Experimental Setup

In Fig. 1(a) the GPRI-II real-aperture terrestrial radar in its standard configuration is shown [2]. For the synthetic aperture radar experiment described here the following modifications were applied to the standard GPRI-II hardware:

1) The long real-aperture antennas were replaced by horn antennas to get a wider beamwidth which is suited for the synthetic aperture radar mode.
2) A different antenna rack was used such that the antennas can be mounted on the roof-top of a car.
3) Accurate positioning and basic attitude information was acquired by means of carrier-phase-based differential GPS measurements at an update rate of 20 Hz.

Interferometric SAR data was acquired along two different roads (curved/straight) at different nearly constant velocities. The example data set presented in this contribution was taken from a slightly curved road at an average speed of $21 m/s$. An overview of the system

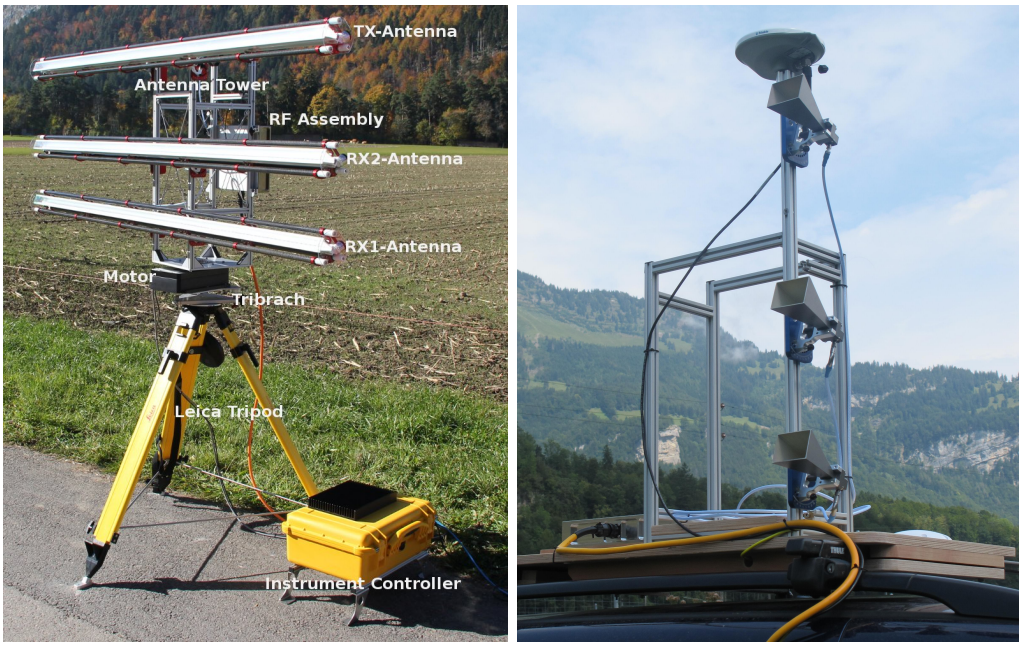

(a) (b)

Fig. 1. (a) GPRI-II standard configuration (terrestrial real-aperture radar). (b) Modified antenna configuration and antenna rack including GPS antennas for accurate positioning as used in the CARSAR experiment.

TABLE I
GPRI-II GROUND BASED RADAR SYSTEM SPECIFICATIONS FOR SYNTHETIC APERTURE RADAR MODE.

Carrier frequency	17.2 GHz
Chirp bandwidth	200 MHz
Type	FMCW
Chirp length	0.001 s
Range 3dB beamwidth	18 deg
Azimuth 3dB beamwidth	16.9 deg
Ground speed	21 m/s
Interferometric baseline	0.25 m
Off-nadir angle	110 deg

parameters for this configuration is given in Table I. Fig. 1(b) shows the modified radar system along with the GPS antennas as mounted on the roof-top of a car during their the synthetic aperture radar experiment.

III. Processing Methods

The linear FMCW-type GPRI-II radar works in dechirp-on-receive mode, thus the received signal $s(t)$ is mixed with the reference signal. This transforms the data to a deramped signal s_d of the form [6]:

$$s_d(t) = s^*(t)exp(j2\pi f_s t + j\pi\gamma t^2), \quad (1)$$

where f_s is the start frequency of the chirp and γ is the chirp rate. The phase of the resulting deramped signal is

$$\varphi_d(t) = (2\pi f_s t_n - \pi\gamma t_n^2) + 2\pi\gamma t_n t, \quad (2)$$

which can be directly related to range distance via a range-Fourier transform. t_n is the two-way time delay to a target n. In contrast to the matched-filter-based range imaging, a range-dependent quadratic phase error (within brackets), known as the residual video phase, remains after this range-compression operation [7]. While for static operation mode—which is the original purpose of the GPRI-II radar—this residual video phase can be neglected it has to be compensated if substantial range-cell migration occurs in the synthetic aperture operation mode.

SAR focusing along the slightly curved sensor trajectory following a main road was performed using a

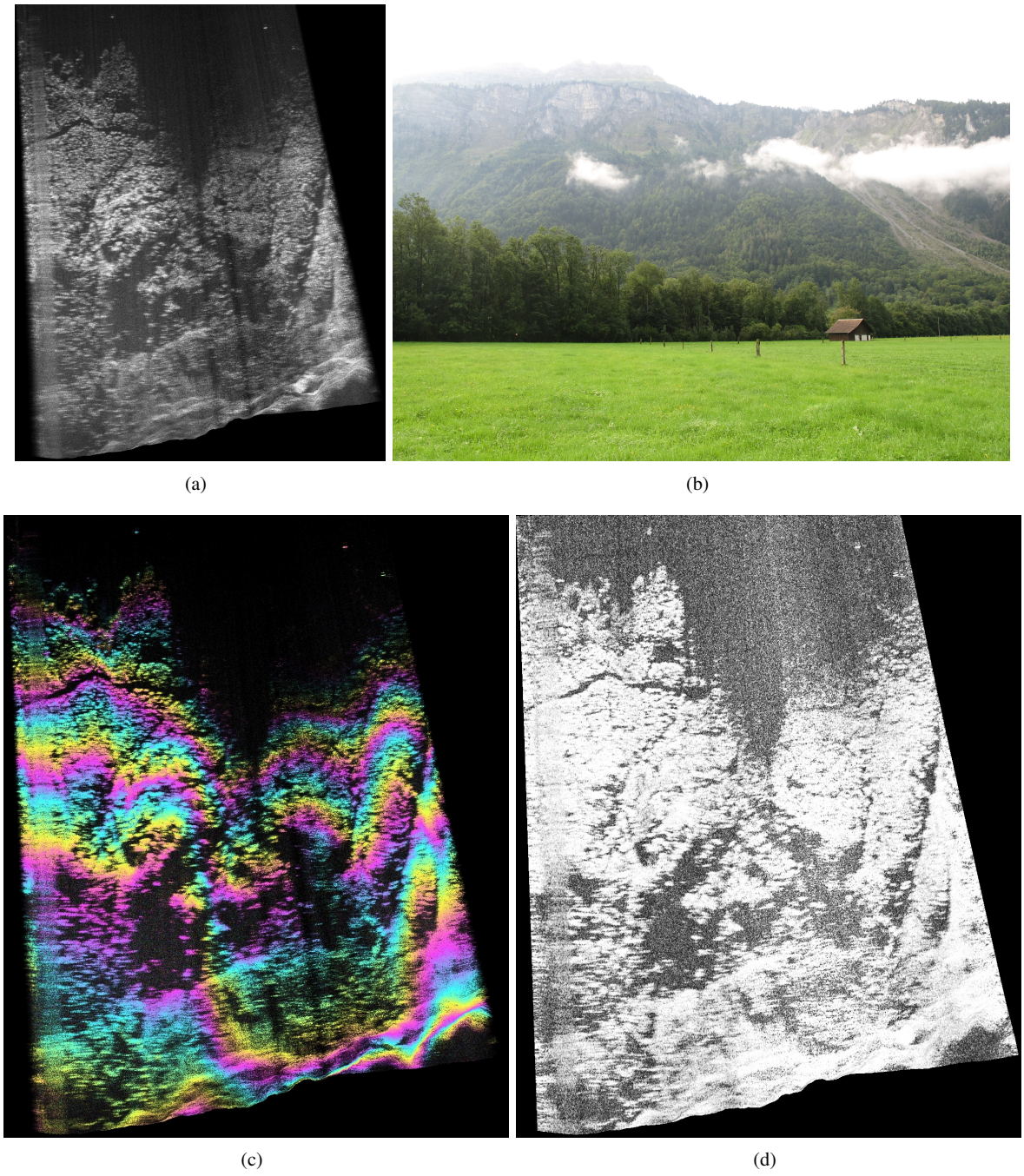

Fig. 2. Example SAR imagery of a slope of a valley taken from the car-borne interferometric SAR system: (a) SAR intensity image, (b) photograph of the imaged slope of the valley, (c) interferogram (blended with intensity image), (d) coherence magnitude.

time-domain back-projection processing approach [8]. Accurate positioning information was obtained by post-processing of carrier-phase-based short-baseline differential GPS data relative to a GPS ad-hoc reference station that was set up on the test site. Due to the long chirp duration of 1 millisecond the start-stop approximation is not valid and therefore the time varying position of the sensor has to be taken into account during back-

projection processing. A detailed treatment of this aspect is found in [9]).

IV. Results

In Fig. 2(a) a focused SAR image taken from the interferometric radar mounted on the roof-top of a car driving along a slightly curved highway is shown. Fig. 2(b) shows a photograph of the valley slope imaged by the car-borne SAR system. Figures 2(c) and 2(d) depict the single-pass interferogram and the coherence magnitude, respectively.

V. Conclusion

A CARSAR experiment using a modified configuration of the Ku-band FMCW GPRI-II terrestrial radar mounted on the roof-top of a car was described. First results of the campaign were presented including focused SAR imagery as well as single-pass interferometry from a slightly curved sensor along a highway demonstrating SAR imaging and single-pass SAR interferometry from an agile car-borne radar system. The SAR and InSAR data takes acquired within this experiment, which includes single-pass and repeat-pass data takes, are being used as a testbed for development and testing of SAR focusing and motion-compensation algorithms and also to evaluate interferometric SAR applications.

References

[1] C. Werner, T. Strozzi, A. Wiesmann, and U. Wegmuller, "A real-aperture radar for ground-based differential interferometry," in *Proc. IEEE Int. Geosci. Remote Sens. Symp.*, vol. 3, July 2008, pp. 210–213.

[2] C. Werner, A. Wiesmann, T. Strozzi, A. Kos, R. Caduff, and U. Wegmuller, "The GPRI multi-mode differential interferometric radar for ground-based observations," in *Proc. EUSAR 2012 - 9th European Conference on Synthetic Aperture Radar*, Apr. 2012, pp. 304–307.

[3] G. Luzi, M. Pieraccini, D. Mecatti, L. Noferini, G. Guidi, F. Moia, and C. Atzeni, "Ground-based radar interferometry for landslides monitoring: atmospheric and instrumental decorrelation sources on experimental data," *IEEE Transactions on Geoscience and Remote Sensing*, vol. 42, no. 11, pp. 2454–2466, Nov. 2004.

[4] D. Leva, G. Nico, D. Tarchi, J. Fortuny-Guasch, and A. Sieber, "Temporal analysis of a landslide by means of a ground-based SAR interferometer," *IEEE Transactions on Geoscience and Remote Sensing*, vol. 41, no. 4, pp. 745–752, Apr. 2003.

[5] T. Strozzi, C. Werner, A. Wiesmann, and U. Wegmuller, "Topography mapping with a portable real-aperture radar interferometer," *IEEE Geosci. Remote Sens. Lett.*, vol. 9, no. 2, pp. 277–281, Mar. 2012.

[6] M. Soumekh, *Synthetic Aperture Radar Signal Processing: with MATLAB Algorithms*. John Wiley & Sons, 1999.

[7] W. G. Carrara, R. S. Goodman, and R. M. Majewski, *Spotlight Synthetic Aperture Radar: Signal Processing Algorithms*. Artech House Inc., 1995.

[8] O. Frey, C. Magnard, M. Rüegg, and E. Meier, "Focusing of airborne synthetic aperture radar data from highly nonlinear flight tracks," *IEEE Trans. Geosci. Remote Sens.*, vol. 47, no. 6, pp. 1844–1858, June 2009.

[9] A. Ribalta, "Time-domain reconstruction algorithms for fmcw-sar," *IEEE Geoscience and Remote Sensing Letters*, vol. 8, no. 3, pp. 396–400, May 2011.